Dalton Transactions

ROYAL SOCIETY OF CHEMISTRY

PAPER

View Article Online
View Journal | View Issue

Open Access Article. Published on 14 November 2023. Downloaded on 10/17/2025 10:39:15 PM.
This article is licensed under a Creative Commons Attribution-NonCommercial 3.0 Unported Licence.

Check for updates

Cite this: *Dalton Trans.*, 2023, **52**, 17873

Vapor-assisted synthesis of the MOF-74 metal–organic framework family from zinc, cobalt, and magnesium oxides†

Nathalie Wauteraerts,[a] Min Tu,[a,b] Nicolas Chanut,[a] Sabina Rodríguez-Hermida,[a,c] Jesus Gandara-Loe[a] and Rob Ameloot *[a]

Received 9th June 2023,
Accepted 31st October 2023

DOI: 10.1039/d3dt01785k

rsc.li/dalton

In this work, we investigate the vapor-assisted synthesis of the metal–organic framework MOF-74 starting from three metal oxides (ZnO, CoO, and MgO). Depending on the nature of the added vapor (H_2O, DMF, DMSO), the metal oxide, and the temperature, the outcome of the reaction can be directed towards the desired porous phase. *Ex situ* and *in situ* XRD measurements reveal the formation of an intermediate phase during the reaction of MgO with H_4dobdc, while the MOF-74 phase forms directly for ZnO and CoO. The reduced CO_2 uptake of the resulting materials compared to solvothermally prepared MOFs might be offset by the convenience of the presented route and the promise of a high space time yield.

Introduction

Metal–organic frameworks (MOFs) are crystalline materials consisting of metal nodes connected by multitopic organic linkers.[1] A high degree of structural and functional tuneability combined with large specific surface areas and porosity position them as interesting materials for gas storage, molecular separation, and catalysis.[2,3] MOFs are typically synthesized *via* solvothermal methods, in a temperature range from room temperature up to 250 °C.[4] For standard solvothermal synthesis recipes, the solvent can make up 40–45% of the production cost on an industrial scale.[5] In addition, the metal salts that are often used to synthesize MOFs can be expensive and yield a stoichiometric amount of waste. When starting from metal oxides, only H_2O is generated as a byproduct.[6] In this perspective, water-based synthesis methods are developed for MOF-74 to eliminate the use of solvents.[7–11] Additionally, the spray-drying technique has been proposed as a green synthesis method which is already applied at pilot-scale.[12] Alternative, solvent-free or solvent-lean routes for MOF synthesis, such as mechanochemical and vapor-phase processes using non-salt metal precursors, can overcome these limitations.[13–16]

In mechanochemical approaches, a chemical reaction is induced by grinding the solid precursors. To achieve MOF materials, inexpensive and readily available metal oxides are often used as precursors. No or little solvent is needed during the process, and water is the sole byproduct. Therefore, it is an environmentally friendly and cost-efficient alternative to solvothermal methods.[14] However, obtaining an open framework *via* neat grinding is difficult and limited to a few materials.[17] In liquid-assisted grinding, a small amount of solvent is added to accelerate the reactions.[17,18] The grinding liquid can affect the nature and crystallinity of the phases that are formed by altering the coordination of the metal nodes.[14,19] An alternative approach without the need for mechanical energy input is vapor-assisted aging, also called vapor digestion or accelerated aging. In that approach, solid reactants are transformed into MOFs in the presence of water or solvent vapor at mild temperatures.[20–26]

The occurrence of multiple polymorphs in several MOF systems can make it difficult to control the synthesis outcome. In solvothermal synthesis methods, fine-tuning the reaction conditions such as precursor concentration, solvent composition, synthesis duration, *etc.*, is often critical to obtain the desired phase.[27] Often, the solvent influences the coordination behavior of the metal ion and/or fills the pores to direct the MOF formation process.[28,29] In a vapor-assisted method, the linker molecule itself or an additive can take up this role.[30,31]

MOF-74 (M_2(dobdc), also called CPO-27) is a promising candidate for H_2 storage and CO_2 capture.[32–36] This MOF material can form with several metal ion nodes (Mg^{2+}, Zn^{2+}, Co^{2+}, Fe^{2+}, Ni^{2+}, Mn^{2+}, Cd^{2+}, Cu^{2+}) connected by 2,5-dihydroxybenzenedi-

[a]*Center for Membrane Separation, Adsorption, Catalysis and Spectroscopy (cMACS), KU Leuven – University of Leuven, Celestijnenlaan 200F, 3001 Leuven, Belgium. E-mail: rob.ameloot@kuleuven.be*
[b]*2020 X-Lab and State Key Laboratory of Transducer Technology, Shanghai Institute of Microsystem and Information Technology, Chinese Academy of Sciences, Shanghai 200050, China*
[c]*Servizos de Apoio á Investigación, Universidade da Coruña, Campus Elviña s/n 15071, A Coruña, Spain*

†Electronic supplementary information (ESI) available: Characterization methods, SEM images, additional X-ray diffractograms, N_2 adsorption isotherms and FTIR spectra plots. See DOI: https://doi.org/10.1039/d3dt01785k

Open Access Article. Published on 14 November 2023. Downloaded on 10/17/2025 10:39:15 PM.
This article is licensed under a Creative Commons Attribution-NonCommercial 3.0 Unported Licence.

carboxylate ($dobdc^{4-}$), resulting in hexagonal channels with a diameter of 11 Å.[37–39] The metal ions are arranged in a five-coordinated square-pyramidal geometry leaving one coordination site open.[32,40–42] In the solvothermal synthesis of MOF-74, the solvent composition and reaction temperature is critical to obtain the desired phase. When DMSO is used instead of the standard DMF–H_2O mixture in the solvothermal synthesis of Zn-MOF-74, a different polymorph, Zn-UTSA-74, is obtained.[43] Performing the Zn-MOF-74 synthesis procedure at 158 °C instead of 105 °C, leads to Zn-UTSA-74 as well.[44] The binuclear secondary building unit of Zn-UTSA-74 comprises one tetrahedrally coordinated metal ion node that is coordinatively saturated and one octahedrally coordinated metal ion node that has two open metal sites as the two water molecules occupying the axial positions can be removed during activation. The resulting structure has a pore aperture of 8 Å, slightly smaller than Zn-MOF-74. Zn-UTSA-74 has shown promising results for the separation of C_2H_2/CO_2,[44] although it converts to Zn-MOF-74 in the presence of liquid water or water vapor.[43] Besides the solvent choice and temperature, the formed topology is determined by the pH. When the reaction environment is not basic enough to deprotonate the hydroxyl groups on the linker, Mg-CPO-26 (Mg(H_2dobdc)(H_2O)$_2$) is formed.[37,45] Only the carboxylate groups of the linker and 2 additional water molecules coordinate to the metal center, forming a non-porous, three-dimensional network.[45] These examples illustrate that predicting the outcome of different synthesis procedures, is challenging and complex in the case of MOF-74.[27,28,37]

Several research groups investigated the mechanochemical synthesis of MOF-74 *via* ball milling. Attempts to synthesize Zn-MOF-74 mechanochemically from ZnO and H_4dobdc (2 : 1) without added liquid did not result in any desired reaction products. However, when H_2O or DMF was added, Zn-MOF-74 was achieved.[13,46] Also, Mg-MOF-74 could be obtained starting from MgO when MeOH assisted the formation. However, for Co-MOF-74, $Co(OAc)_2{\cdot}4H_2O$ was needed as a precursor and DMF was added.[47] Wang *et al.* showed that M-MOF-74 (M = Mg, Mn, Co, Ni, Cu, and Zn) could also be achieved starting from metal nitrate salts through liquid-assisted grinding when an organic base, *N*,*N*-diisopropylethyleneamine, was added to deprotonate the linker and facilitate grinding.[48] Finally, Ayoub *et al.* investigated the mechanochemical synthesis of mixed-metal MOF-74 starting from pre-assembled complexes of Zn^{2+}, Mg^{2+}, Ni^{2+}, and Co^{2+}.[47] At last, increasing the reaction temperature can accelerate the reaction significantly. At room temperature, the conversion reaction of ZnO : H_4dobdc (2 : 1) in the presence of H_2O is not finished after 24 hours of ball-milling. However, at 75 °C, only 8 minutes are needed to complete the conversion.[13,49] In all these cases, ball milling was necessary to achieve the MOF; no vapor-assisted aging procedure exists for MOF-74. The development of such a method would allow the green synthesis of MOF-74 without the need for a ball mill.

This paper reports the formation of M-MOF-74 (M = Mg, Zn, Co) by a vapor-assisted method starting from metal oxide precursors. To enable the formation of the desired MOF-74 phase, it was necessary to introduce an additive (H_2O, DMF, or DMSO) in the vapor phase and control the temperature. Different templating effects were observed depending on the structural metal ion. The conversion was monitored by *in situ* and *ex situ* diffraction measurements (Scheme 1).

Experimental

Materials

MgO (98+%, <45 μm, Acros Organics); ZnO (99.5+%, <5 μm, Carl Roth); CoO (74+%, <45 μm, Acros Organics); H_4dobdc (98%, Sigma-Aldrich); *N*,*N*-dimethyl formamide (99+%, extra pure, Acros Organics); dimethyl sulfoxide (99.7+%, Acros Organics); *N*,*N*-diethylformamide (99%, Acros Organics); *N*,*N*-dimethylacetamide (extra pure 99.5%, Acros Organics).

Synthesis of M_2dobdc

Metal oxide (ZnO, 61.6 mg; MgO, 30.5 mg; CoO 56.7 mg) was mixed with 75 mg H_4dobdc (molar ratio 2 : 1) with a mortar and pestle until the mixture was visually homogeneous. Afterwards, the mixture was placed in a 25 ml Schott bottle. The additive (<50 μL) was put in a separate 2 mL vial and placed inside the Schott bottle. The Schott bottle was sealed and placed in preheated oven with a temperature in the range of 100–150 °C for 24 h. Afterwards, the samples were washed *via* soxhlet extraction with methanol for 24 h. Reference Zn-MOF-74 was synthesized according to published procedure.[11] The characterization data of the as-synthesized MOF materials through powder X-ray diffraction (PXRD), thermogravimetric analysis (TGA), scanning electron microscopy (SEM), FTIR spectroscopy, N_2 and CO_2 adsorption can be found in the ESI.†

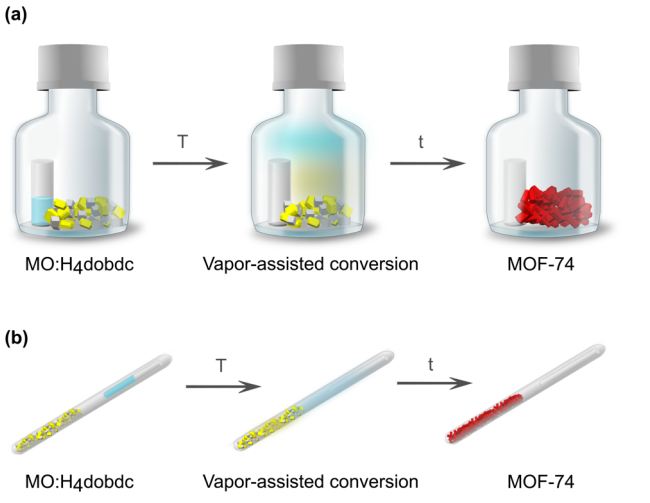

Scheme 1 Setups for the vapor-assisted synthesis of MOF-74: metal oxide (MO) and H_4dobdc linker are mixed in a 2 : 1 ratio. (a) Setup for *ex situ* MOF-74 synthesis. The physical mixture is placed in a 25 ml bottle together with a vial containing an additive. (b) Setup for *in situ* XRD measurements to monitor the vapor-assisted synthesis of MOF-74. The physical mixture is inserted into a 1.0 mm diameter capillary. Afterwards, a smaller capillary (diameter 0.7 mm) containing a small amount of additive is inserted and the outer capillary is sealed (Fig. S1†).

 This journal is © The Royal Society of Chemistry 2023

Open Access Article. Published on 14 November 2023. Downloaded on 10/17/2025 10:39:15 PM.
This article is licensed under a Creative Commons Attribution-NonCommercial 3.0 Unported Licence.

Results and discussion

When a metal oxide (MgO, ZnO, CoO) and H_4dobdc were heated together to 150 °C without an additive, no reaction occurred. In contrast, by introducing humidity, M-MOF-74 (M = Mg, Co) could be obtained through the conversion of MgO or CoO with H_4dobdc in a temperature range of 100–150 °C with conversion times of up to 24 h (Scheme 2 and Fig. S2†). The resulting crystallites had a rod-shaped structure growing in floret-like groups and reaching lengths of several µm (Fig. S3 and S4†). The volume of added water was controlled to reach a partial pressure 0.2 bar below the saturation pressure to prevent condensation. In the case of MgO, the non-porous phase Mg-CPO-26 (CCDC: VOGTER) was observed when the partial pressure of water exceeds the saturation pressure and condensation occurs (Fig. S5 and S6†).

When ZnO and H_4dobdc reacted in a humid atmosphere, a dense coordination polymer (CP) was formed: $[Zn(H_2O)_2(H_2dobdc)]_n$, which is further referred to as CP-ZnH_2dobdc. This structure did not transform into the open MOF-74 structure upon further heating in the presence of H_2O vapor. Likely, the different behavior of ZnO is due to its lower basicity compared to CoO and MgO, making it less reactive.[50] In the formation of CP-ZnH_2dobdc, only the carboxylic acid groups of the H_4dobdc linker are deprotonated while the phenolic hydroxyls remain protonated, thus preventing the formation of MOF-74.

The formation of Mg-MOF-74 in the presence of H_2O vapor was investigated by *in situ* diffraction measurements at DESY beamline P02.1 (Fig. S7†). These measurements revealed an intermediate phase present at the start, which was converted to Mg-MOF-74 upon heating to 130 °C (Fig. 1c). The intermediate phase, $Mg(H_2dobdc)(H_2O)_5{\cdot}H_2O$, is a hydrogen-bonded 3D structure built from mononuclear (MN) units consisting of 5 H_2O molecules and one $dobdc^{2-}$ anion coordinated to a Mg^{2+} ion, and will be further referred to as MN-MgH_2dobdc.[51] The same structure was obtained by Henkelis *et al.* as a by-product of Mg-MOF-74 synthesis after evaporation of the remaining solvent at room temperature.[51] This structure was also observed *ex situ* when the reaction proceeded at 50 °C (Fig. S8 and S9†). This dense phase transforms upon heating into the more thermodynamically stable product, Mg-MOF-74.[52] This transformation is in line with earlier observations that a higher synthesis temperature favors the transition from a 2D to 3D framework.[27,53,54]

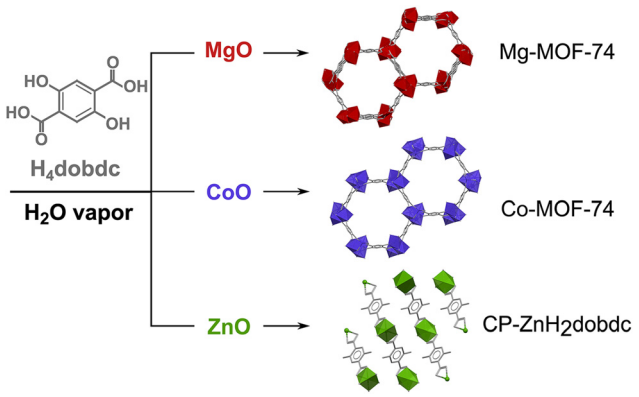

Scheme 2 Products obtained by the reaction of different metal oxides with H_4dobdc in a humid atmosphere at 130 °C. For MgO and CoO, MOF-74 is obtained (CCDC: VOGTIV and ORIWAP, respectively). ZnO yields a dense coordination polymer $[Zn(H_2O)_2(H_2dobdc)]_n$ (CCDC: ODIPOH01).

Synchrotron SAXS measurements were performed to investigate the effect of the reaction temperature on Mg- and Co-MOF-74 (Fig. 1). At 100 °C (Fig. 1a), Mg-MOF-74 could be observed after 10 minutes, following an initial growth phase of MN-MgH_2dobdc. The content of the latter phase diminished rapidly once MOF-74 started to form, and continued decreasing until the end of the measurement (45 minutes). In contrast, at 130 °C (Fig. 1b), the transformation of MN-MgH_2dobdc into MOF-74 already started after 3 minutes and was completed after only half a minute.

When CoO reacted with the linker in the presence of humidity, it transformed into Co-MOF-74 without forming an intermediate phase (Fig. 1d). At 100 °C, the conversion initiated after 7 minutes, slightly faster than for the Mg-analog. The vapor-assisted synthesis of Mg- and Co-MOF-74 can also be observed *via* the color change of the precursor mixtures. The color changes from light to dark yellow in the case of Mg-MOF-74, and from light yellow to brown for Co-MOF-74 (Fig. S10†).

The reaction of ZnO with H_4dobdc in a humid atmosphere does not result in Zn-MOF-74, as indicated above. Therefore, we introduced other vapor additives to direct the reaction towards Zn-MOF-74 (Scheme 3). DMF and DMSO have already proven to template the vapor-assisted synthesis of other porous MOF materials.[30,31] In contrast to H_2O, DMF vapor steers the reaction towards the desired Zn-MOF-74 phase (Fig. S11a and S12†). The study by Henkelis *et al.* shows that different molecules occupy the open metal sites in the as-synthesized MOF structure for the Mg^{2+} and Zn^{2+} variants based on single-crystal XRD analysis. For Mg-MOF-74, H_2O is coordinated to the metal sites, while DMF is preferentially coordinating in Zn-MOF-74.[55] This observation suggests that these molecules can play a structure-directing role in the formation of the respective MOFs. In addition, DMF can partially decompose to formic acid and dimethylamine during MOF synthesis at elevated temperatures. Dimethylamine is a weak base (pK_b = 3.3) but can deprotonate the carboxyl groups of the H_4dobdc linker ($pK_a < 5$).[56]

When DMF vapor is used to obtain Zn-MOF-74, the reaction temperature plays a critical role. At lower temperatures, only Zn-MOF-74 is formed. By increasing the reaction temperature, Zn-UTSA-74 can be observed (Fig. 2). At 150 °C, UTSA-74 is the only reaction product. This temperature effect is in agreement with the synthesis procedure by Luo *et al.*, in which Zn-UTSA-74 is obtained at higher temperatures (158 °C) compared to Zn-MOF-74 (105 °C).[39,44] The observation that Zn-UTSA-74 is preferred at higher temperatures might be explained by the

Open Access Article. Published on 14 November 2023. Downloaded on 10/17/2025 10:39:15 PM.
This article is licensed under a Creative Commons Attribution-NonCommercial 3.0 Unported Licence.

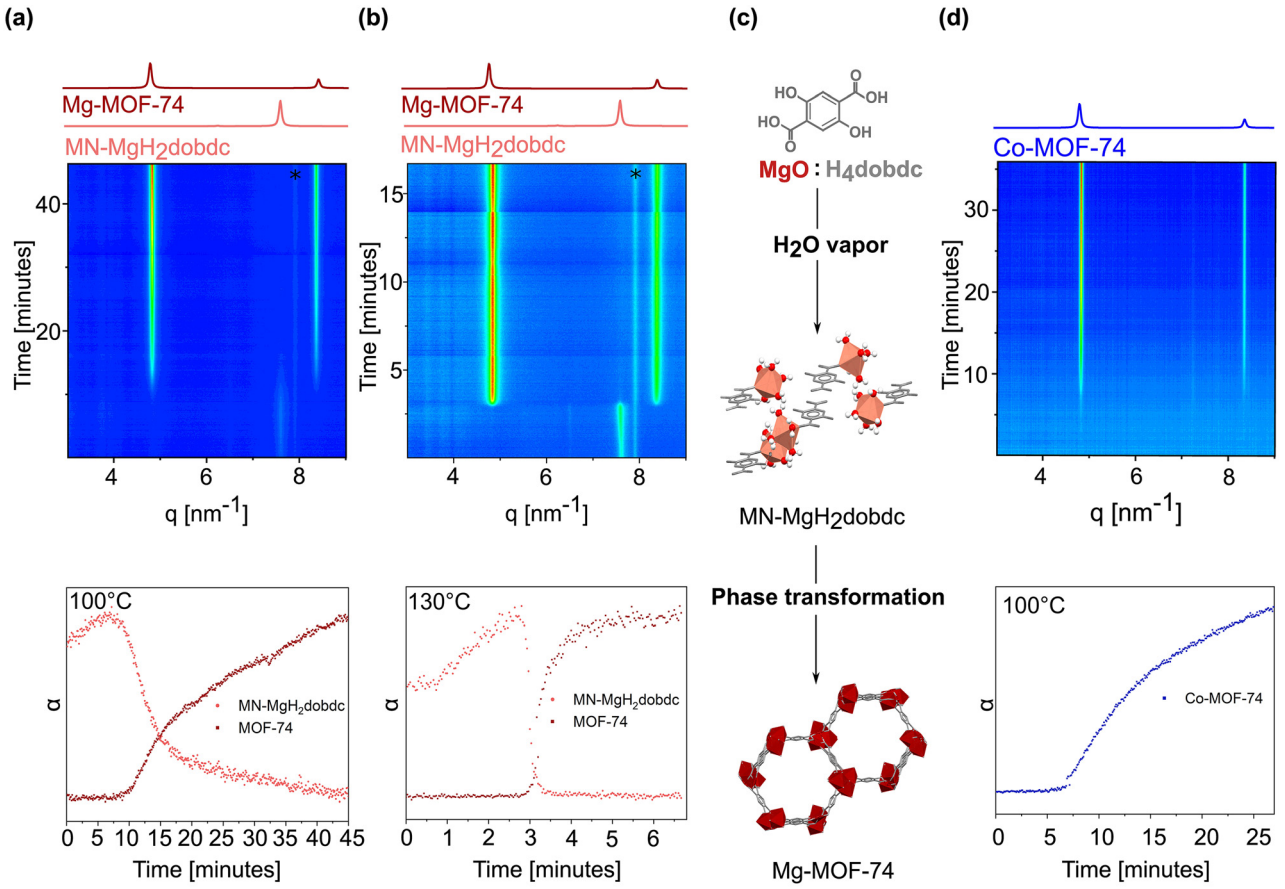

Fig. 1 Vapor-assisted formation of Mg-MOF-74 and Co-MOF-74 starting from respectively MgO and CoO with H_4dobdc in the presence of H_2O vapor. Top: *In situ* SAXS measurements (SAXS beamline Elettra Synchrotron) at different temperatures: (a) Mg-MOF-74 at 100 °C, (b) Mg-MOF-74 at 130 °C and (d) Co-MOF-74 at 100 °C. The asterisk corresponds to parasitic scattering of the set-up. Bottom: Extent of reaction (α) as function of time determined by the integrated peak intensities of the (1 0 1) reflection of MN-MgH_2dobdc at q = 7.8 nm^{-1} and the (2 −1 0) reflection of MOF-74 at q = 4.8 nm^{-1}. (c) Schematic illustration of the stepwise formation of Mg-MOF-74 with the structures of H_4dobdc, MN-Mg-H_2dobdc (CCDC: XAJGEX) and Mg-MOF-74 (CCDC: VOGTIV).

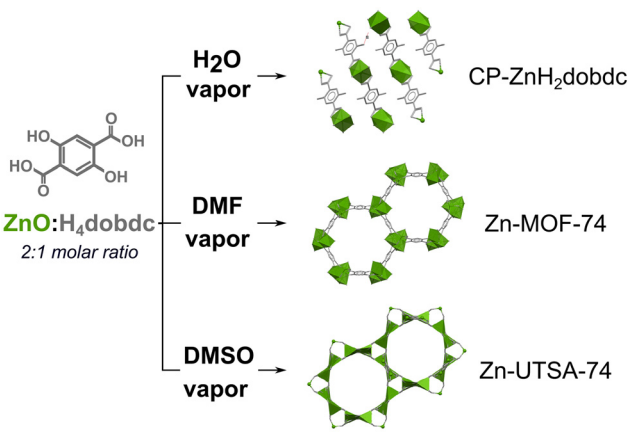

Scheme 3 Products obtained by the reaction of ZnO with H_4dobdc in the presence of different vapor additives: in the presence of H_2O vapor, the dense coordination polymer $[Zn(H_2O)_2(H_2dobdc)]_n$ (CCDC: ODIPOH01) is obtained. In the presence of DMF vapor, Zn-MOF-74 (CCDC: ORIVOC) is formed. When DMSO vapor is introduced, UTSA-74 (CCDC: OLEYAH) is obtained.

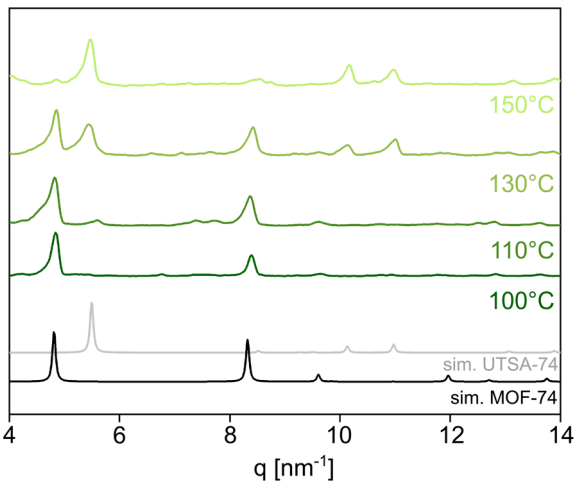

Fig. 2 Diffractograms of the reaction products of ZnO with H_4dobdc in the presence of DMF at different temperatures. At a lower temperature (100 °C) Zn-MOF-74 is preferentially formed and at a higher temperature (150 °C) Zn-UTSA-74.

 This journal is © The Royal Society of Chemistry 2023

Open Access Article. Published on 14 November 2023. Downloaded on 10/17/2025 10:39:15 PM.
This article is licensed under a Creative Commons Attribution-NonCommercial 3.0 Unported Licence.

increased presence of dimethylamine at elevated temperatures, which affects the rate of linker deprotonation and can modify the coordination environment of the metal ions.[56] This hypothesis is supported by the formation of Zn-UTSA-74 in the presence N-donor modulators at a temperature typically used to synthesize Zn-MOF-74 (120 °C).[57,58]

Co-MOF-74 can also be formed upon reaction of CoO and H_4dobdc in the presence of DMF vapor. CoO directly converts into Co-MOF-74 at 150 °C (Fig. S13†), as in the case when H_2O vapor is present. However, at 50 °C in the presence of DMF vapor, an additional phase, $Co(dobdc)(DMF)_2(H_2O)_2$ (CCDC: SEWXIE), is formed (Fig. S14 and S15†). In this dense phase, Co^{2+} is octahedrally coordinated to 2 H_2O molecules, 2 carboxylate groups of the linker, and 2 DMF molecules.[59] In the case of MgO, DMF vapor does not direct the synthesis of Mg-MOF-74. An unknown phase can be observed (Fig. S12†).

In the presence of DMSO vapor, ZnO is converted into Zn-UTSA-74 (Fig. S16 and S11b†). The structure-directing effect of DMSO, likely through the stabilization of the dimer SBUs,[43] is in agreement with a report by Bueken *et al.* in which Zn-UTSA-74 is formed instead of Zn-MOF-74 when DMSO is used as the reaction solvent. The reaction products for the Mg and Co variants in the presence of DMSO vapor are unknown crystalline phases (Fig. S16†).

The thermal stability and compositional purity of the different materials were investigated by TGA after washing with methanol (Fig. 3). The TGA curves show the same weight loss steps as previously reported.[47,60–62] First, (30–150 °C) is attributed to the removal of solvent (MeOH) and H_2O molecules. In a second step, the framework starts to collapse and decomposes above 200 °C. From TGA measurements under air, we can calculate the weight loss attributed to the MOF framework by comparing the theoretical weight loss with the experimental one (Table S1†). From these results, it can be concluded that full conversion is reached for the 3 samples.

To demonstrate the porosity and the potential of these materials for CO_2 capture, N_2 and CO_2 adsorption isotherms were recorded after activation at 150 °C for 12 h under vacuum (Fig. 4 and S17†). BET surface areas of 313, 290 and 285 m^2 g^{-1} were measured for Mg-, Co- and Zn-MOF-74, respectively. These values are significantly lower compared to those previously reported (Table S3†). Mg-MOF-74 showed the highest and steepest CO_2 uptake of 2.55 mmol g^{-1} at 1.15 bar followed by Co-MOF-74 (2.37 mmol g^{-1}) and Zn-MOF-74 (1.87 mmol g^{-1}). However, the same level of CO_2 uptake as resulting from another synthesis method is not reached (Fig. S18†). On average, 30% of the reported CO_2 capacity is reached. An overview of CO_2 adsorption data in literature is given in Table S2.† As the experimental weight loss only slightly deviates from the theoretical one, it can be assumed that the loss in CO_2 uptake is not caused solely by incomplete conversion of the precursors. The study of Liang *et al.* shows that activation at 150 °C under vacuum is sufficient to reach 90% of the available pore volume. Additional activation up to 300 °C is necessary to remove all the coordinated molecules.[61] However, in our case, a higher activation temperature (200 °C) did not lead to an increase in CO_2 uptake.

Quantitative analysis of the powder X-ray diffractograms (Fig. S19†) showed that the amount of MOF-74 present in the vapor-assisted synthesized sample is largely reduced (<50%) in comparison to hydrothermally synthesized MOF-74. This indicates that non-porous, amorphous impurities with a similar composition and thermal stability as MOF-74 are present. The reduction in crystalline content matches the reduction of CO_2 uptake (45%).

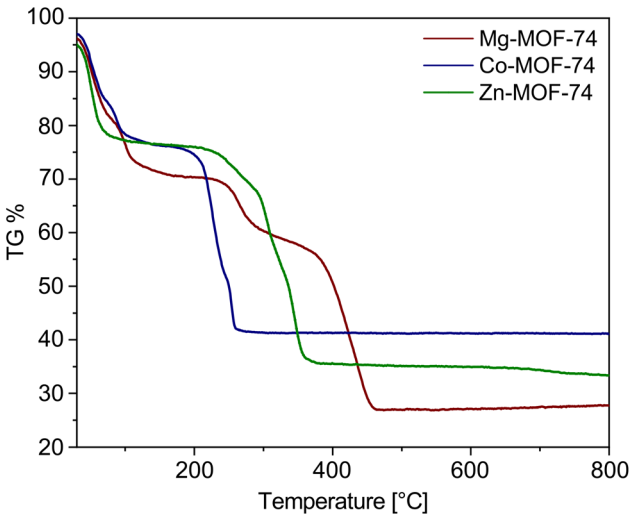

Fig. 3 TGA measurements of M_2(dobdc) (M = Mg, Zn and Co) under air atmosphere (20% O_2 and 80% N_2) with a heating rate of 1 °C min^{-1}. Red line represents Mg-MOF-74, blue line represents Co-MOF-74 and green line represents Zn-MOF-74.

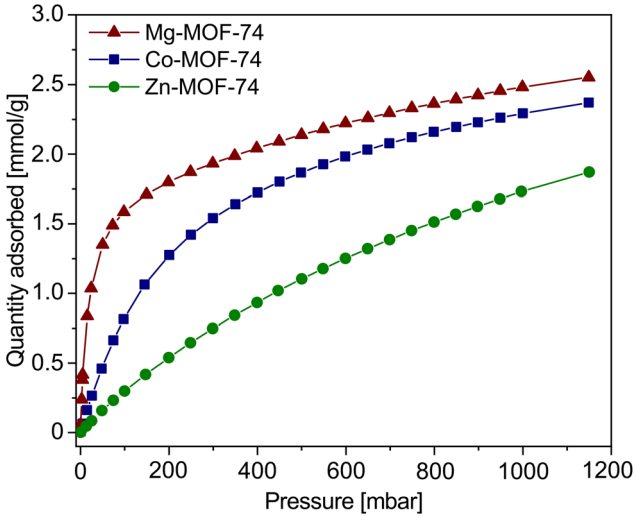

Fig. 4 CO_2 adsorption isotherms for M_2(dobdc) (M = Mg, Zn and Co) recorded at 25 °C. Red line with triangles represents Mg-MOF-74, blue line with squares represents Co-MOF-74 and green line with circles represents Zn-MOF-74.

Open Access Article. Published on 14 November 2023. Downloaded on 10/17/2025 10:39:15 PM.
This article is licensed under a Creative Commons Attribution-NonCommercial 3.0 Unported Licence.

Additionally, very long measurement times were recorded for N_2 and CO_2 adsorption in MOF-74 samples synthesized by the vapor-assisted method. In addition to the intrinsic lower uptake of the materials obtained through the vapor-assisted approach, the much slower uptake kinetics of these samples might have prevented the measurements from reaching equilibrium in the low pressure region, thereby reducing the apparent N_2 uptake and the surface area.[63] Likely, this behavior is caused by pore blocking by the amorphous phase.[64]

From these results, we can conclude that the reduced CO_2 and N_2 uptake of the MOF-74 samples synthesized by the vapor-assisted method originates from the presence of non-crystalline material.[65,66] Although the linkers are mainly present in a coordinated fashion (Fig. S20†), at least through their carboxylate groups, it is likely that the amorphous phase partially blocks the pores. As a result, the uptake capacity is lowered and the uptake kinetics are slowed down.

From capillary measurements, we can see that full conversion is reached after 6 minutes. In this way a few mg of material is obtained in the limited volume of a capillary (±20 mm^3). As the reported method shows promising results to achieve a high space time yield (STY) in contrast with solvothermal methods, future work will focus on improving the crystallinity and therefore the CO_2 uptake *via* the vapor-assisted approach.

Conclusions

In conclusion, this work demonstrates the vapor-assisted synthesis of the M-MOF-74 family (M = Mg, Co, Zn). Different polymorphs are obtained depending on the nature of additive vapors in combination with the coordination preferences of the metal ions. The results emphasize the importance of *in situ* diffraction measurements for vapor-assisted synthesis methods to better understand the vapor-assisted conversion. To conclude, vapor-assisted synthesis enables obtaining promising MOF materials in an environmentally benign way without the need for bulk solvents or a mechanochemical reactor.

Author contributions

N. W., M. T., and R. A. designed the experiments. N. W. conceived the experiments. S. R. assisted during *in situ* XRD measurements. N. C. performed CO_2 adsorption measurements. J. G. L. performed FTIR measurements. N. W. drafted the manuscript and all authors contributed to revising the manuscript.

Conflicts of interest

There are no conflicts to declare.

Acknowledgements

The authors acknowledge the funding by the Research Foundation Flanders (FWO Vlaanderen) in research projects G087422N and G085720N, and the funding by KU Leuven in research project C14/20/085. N. W. acknowledges FWO for PhD fellowships (1SB7921N and 1SB7919N). M. T. acknowledges financial support by the National Key R&D Program of China (2021YFB3200800). We acknowledge the Elettra Synchrotron (Trieste, Italy) for allocation of beamtime at 5.2L SAXS beamline (NFFA: ID-1025) and Heinz Amenitsch for his guidance. We acknowledge DESY (Hamburg, Germany), for the allocation of beamtime at P02.1 beamline (I-20180033 EC) and Michael Wharmby for his guidance.

Notes and references

1 S. R. Batten, N. R. Champness, X.-M. Chen, J. Garcia-Martinez, S. Kitagawa, L. Ohrstrom, M. O'Keeffe, M. P. Suh and J. Reedijk, *Pure Appl. Chem.*, 2013, **85**, 1715–1724.
2 H. Li, K. Wang, Y. Sun, C. T. Lollar, J. Li and H.-C. Zhou, *Mater. Today*, 2018, **21**, 108–121.
3 M. Ranocchiari and J. A. van Bokhoven, *Phys. Chem. Chem. Phys.*, 2011, **13**, 6388–6396.
4 N. Stock and S. Biswas, *Chem. Rev.*, 2012, **112**, 933–969.
5 D. DeSantis, J. A. Mason, B. D. James, C. Houchins, J. R. Long and M. Veenstra, *Energy Fuels*, 2017, **31**, 2024–2032.
6 J. Chen, K. Shen and Y. Li, *ChemSusChem*, 2017, **10**, 3165–3187.
7 S. Cadot, L. Veyre, D. Luneau, D. Farrusseng and E. A. Quadrelli, *J. Mater. Chem. A*, 2014, **2**, 17757–17763.
8 M. Sánchez-Sánchez, N. Getachew, K. Díaz, M. Díaz-García, Y. Chebude and I. Díaz, *Green Chem.*, 2015, **17**, 1500–1509.
9 N. E. Ghermani, G. Morgant, J. d'Angelo, D. Desmaële, B. Fraisse, F. Bonhomme, E. Dichi and M. Sgahier, *Polyhedron*, 2007, **26**, 2880–2884.
10 L. Garzón-Tovar, A. Carné-Sánchez, C. Carbonell, I. Imaz and D. Maspoch, *J. Mater. Chem. A*, 2015, **3**, 20819–20826.
11 D. Cattaneo, S. J. Warrender, M. J. Duncan, R. Castledine, N. Parkinson, I. Haley and R. E. Morris, *Dalton Trans.*, 2015, **45**, 618–629.
12 J. Troyano, C. Çamur, L. Garzón-Tovar, A. Carné-Sánchez, I. Imaz and D. Maspoch, *Acc. Chem. Res.*, 2020, **53**, 1206–1217.
13 P. A. Julien, K. Užarević, A. D. Katsenis, S. A. J. Kimber, T. Wang, O. K. Farha, Y. Zhang, J. Casaban, L. S. Germann, M. Etter, R. E. Dinnebier, S. L. James, I. Halasz and T. Friščić, *J. Am. Chem. Soc.*, 2016, **138**, 2929–2932.
14 T. Friščić and L. Fábián, *CrystEngComm*, 2009, **11**, 743–745.
15 I. Stassen, M. Styles, G. Grenci, H. V. Gorp, W. Vanderlinden, S. D. Feyter, P. Falcaro, D. D. Vos, P. Vereecken and R. Ameloot, *Nat. Mater.*, 2016, **15**, 304–310.

 This journal is © The Royal Society of Chemistry 2023

Open Access Article. Published on 14 November 2023. Downloaded on 10/17/2025 10:39:15 PM.
This article is licensed under a Creative Commons Attribution-NonCommercial 3.0 Unported Licence.

16 T. Stassin, S. Rodríguez-Hermida, B. Schrode, A. J. Cruz, F. Carraro, D. Kravchenko, V. Creemers, I. Stassen, T. Hauffman, D. D. Vos, P. Falcaro, R. Resel and R. Ameloot, *Chem. Commun.*, 2019, **55**, 10056–10059.
17 C.-A. Tao and J.-F. Wang, *Crystals*, 2021, **11**, 15.
18 S. L. James, C. J. Adams, C. Bolm, D. Braga, P. Collier, T. Friščić, F. Grepioni, K. D. M. Harris, G. Hyett, W. Jones, A. Krebs, J. Mack, L. Maini, A. G. Orpen, I. P. Parkin, W. C. Shearouse, J. W. Steed and D. C. Waddell, *Chem. Soc. Rev.*, 2011, **41**, 413–447.
19 T. Stolar, L. Batzdorf, S. Lukin, D. Žilić, C. Motillo, T. Friščić, F. Emmerling, I. Halasz and K. Užarević, *Inorg. Chem.*, 2017, **56**, 6599–6608.
20 X. Feng, C. Jia, J. Wang, X. Cao, P. Tang and W. Yuan, *Green Chem.*, 2015, **17**, 3740–3745.
21 C. Jia, J. Wang, X. Feng, Q. Lin and W. Yuan, *CrystEngComm*, 2014, **16**, 6552–6555.
22 C. Mottillo, Y. Lu, M.-H. Pham, M. J. Cliffe, T.-O. Do and T. Friščić, *Green Chem.*, 2013, **15**, 2121–2131.
23 P. Tang, C. Jia, Y. Jiang, W. Gong, X. Cao, J. Yang and W. Yuan, *Eur. J. Inorg. Chem.*, 2016, 5617–5622.
24 M. J. Cliffe, C. Mottillo, R. S. Stein, D.-K. Bučar and T. Friščić, *Chem. Sci.*, 2012, **3**, 2495–2500.
25 F. Qi, R. S. Stein and T. Friščić, *Green Chem.*, 2013, **16**, 121–132.
26 C. Mottillo and T. Friščić, *Molecules*, 2017, **22**, 144.
27 R. Seetharaj, P. V. Vandana, P. Arya and S. Mathew, *Arabian J. Chem.*, 2019, **12**, 295–315.
28 D. Banerjee, J. Finkelstein, A. Smirnov, P. M. Forster, L. A. Borkowski, S. J. Teat and J. B. Parise, *Cryst. Growth Des.*, 2011, **11**, 2572–2579.
29 F. Israr, D. Chun, Y. Kim and D. K. Kim, *Ultrason. Sonochem.*, 2016, **31**, 93–101.
30 D. E. Kravchenko, A. J. Cruz, S. Rodríguez-Hermida, N. Wauteraerts, T. Hauffman and R. Ameloot, *Chem. Mater.*, 2020, **32**, 10469–10475.
31 M. Tu, D. E. Kravchenko, B. Xia, V. Rubio-Giménez, N. Wauteraerts, R. Verbeke, I. F. J. Vankelecom, T. Stassin, W. Egger, M. Dickmann, H. Amenitsch and R. Ameloot, *Angew. Chem., Int. Ed.*, 2021, **60**, 7553–7558.
32 P. D. C. Dietzel, B. Panella, M. Hirscher, R. Blom and H. Fjellvåg, *Chem. Commun.*, 2006, 959–961.
33 L. Lei, Y. Cheng, C. Chen, M. Kosari, Z. Jiang and C. He, *J. Colloid Interface Sci.*, 2022, **612**, 132–145.
34 S. R. Caskey, A. G. Wong-Foy and A. J. Matzger, *J. Am. Chem. Soc.*, 2008, **130**, 10870–10871.
35 T. Xiao and D. Liu, *Microporous Mesoporous Mater.*, 2019, **283**, 88–103.
36 A. R. Millward and O. M. Yaghi, *J. Am. Chem. Soc.*, 2005, **127**, 17998–17999.
37 P. D. C. Dietzel, R. Blom and H. Fjellvåg, *Eur. J. Inorg. Chem.*, 2008, 3624–3632.
38 T.-T. Zheng, J. Zhao, Z.-W. Fang, M.-T. Li, C.-Y. Sun, X. Li, X.-L. Wang and Z.-M. Su, *Dalton Trans.*, 2017, **46**, 2456–2461.
39 N. L. Rosi, J. Kim, M. Eddaoudi, B. Chen, M. O'Keeffe and O. M. Yaghi, *J. Am. Chem. Soc.*, 2005, **127**, 1504–1518.
40 W. L. Queen, E. D. Bloch, C. M. Brown, M. R. Hudson, J. A. Mason, L. J. Murray, A. J. Ramirez-Cuesta, V. K. Peterson and J. R. Long, *Dalton Trans.*, 2012, **41**, 4180–4187.
41 P. A. Wood, A. A. Sarjeant, A. A. Yakovenko, S. C. Ward and C. R. Groom, *Chem. Commun.*, 2016, **52**, 10048–10051.
42 W. L. Queen, M. R. Hudson, E. D. Bloch, J. A. Mason, M. I. Gonzalez, J. S. Lee, D. Gygi, J. D. Howe, K. Lee, T. A. Darwish, M. James, V. K. Peterson, S. J. Teat, B. Smit, J. B. Neaton, J. R. Long and C. M. Brown, *Chem. Sci.*, 2014, **5**, 4569–4581.
43 B. Bueken, H. Reinsch, N. Heidenreich, A. Vandekerkhove, F. Vermoortele, C. E. A. Kirschhock, N. Stock, D. D. Vos and R. Ameloot, *CrystEngComm*, 2017, **19**, 4152–4156.
44 F. Luo, C. Yan, L. Dang, R. Krishna, W. Zhou, H. Wu, X. Dong, Y. Han, T.-L. Hu, M. O'Keeffe, L. Wang, M. Luo, R.-B. Lin and B. Chen, *J. Am. Chem. Soc.*, 2016, **138**, 5678–5684.
45 P. C. Dietzel, R. Blom and H. Fjellvåg, *Z. Anorg. Allg. Chem.*, 2009, **635**, 1953–1958.
46 J. Beamish-Cook, K. Shankland, C. A. Murray and P. Vaqueiro, *Cryst. Growth Des.*, 2021, **21**, 3047–3055.
47 G. Ayoub, B. Karadeniz, A. J. Howarth, O. K. Farha, I. Đilović, L. S. Germann, R. E. Dinnebier, K. Užarević and T. Friščić, *Chem. Mater.*, 2019, **31**, 5494–5501.
48 Z. Wang, Z. Li, M. Ng and P. J. Milner, *Dalton Trans.*, 2020, **49**, 16238–16244.
49 N. Cindro, M. Tireli, B. Karadeniz, T. Mrla and K. Užarević, *ACS Sustainable Chem. Eng.*, 2019, **7**, 16301–16309.
50 J. C. Lavalley, *Catal. Today*, 1996, **27**, 377–401.
51 S. E. Henkelis, L. J. McCormick, D. B. Cordes, A. M. Z. Slawin and R. E. Morris, *Inorg. Chem. Commun.*, 2016, **65**, 21–23.
52 S.-J. Lee, J. L. Mancuso, K. N. Le, C. D. Malliakas, Y.-S. Bae, C. H. Hendon, T. Islamoglu and O. K. Farha, *ACS Mater. Lett.*, 2020, **2**, 499–504.
53 P. Mahata, A. Sundaresan and S. Natarajan, *Chem. Commun.*, 2007, 4471–4473.
54 Y.-X. Sun and W.-Y. Sun, *Chin. Chem. Lett.*, 2014, **25**, 823–828.
55 S. E. Henkelis, S. M. Vornholt, D. B. Cordes, A. M. Z. Slawin, P. S. Wheatley and R. E. Morris, *CrystEngComm*, 2019, **21**, 1857–1861.
56 O. M. Yaghi, M. J. Kalmutzki and C. S. Diercks, *Introduction to Reticular Chemistry*, John Wiley & Sons, Ltd, 2019, pp. 57–81.
57 A. Gheorghe, I. Imaz, J. I. van der Vlugt, D. Maspoch and S. Tanase, *Dalton Trans.*, 2019, **48**, 10043–10050.
58 H. Yang, J. Le, A. Dinh, X. Zhao, X. Chen, F. Peng, P. Feng and X. Bu, *Chem. – Eur. J.*, 2019, **25**, 10590–10593.
59 L. S. Flores, S. P. Alcântara, G. C. G. de Lima, M. I. Yoshida and C. C. Corrêa, *Vib. Spectrosc.*, 2016, **86**, 302–310.
60 J. Hu, L. Li, H. Li, Y. Zhai, F. Tang, Z. Zhang and B. Chen, *RSC Adv.*, 2022, **12**, 33716–33724.

Open Access Article. Published on 14 November 2023. Downloaded on 10/17/2025 10:39:15 PM.
This article is licensed under a Creative Commons Attribution-NonCommercial 3.0 Unported Licence.

61 X. Liang, P. Wang, C. Li, M. Yuan, Q. Shi and J. Dong, *Microporous Mesoporous Mater.*, 2021, **320**, 111109.
62 A. A. Godoy, D. Villarroel-Rocha, J. J. Arroyo-Gómez, C. Bernini, G. Narda and K. Sapag, *Materials*, 2023, **16**, 117.
63 M. Thommes, K. Kaneko, A. V. Neimark, J. P. Olivier, F. Rodriguez-Reinoso, J. Rouquerol and K. S. W. Sing, *Pure Appl. Chem.*, 2015, **87**, 1051–1069.
64 C. H. Sharp, B. C. Bukowski, H. Li, E. M. Johnson, S. Ilic, A. J. Morris, D. Gersappe, R. Q. Snurr and J. R. Morris, *Chem. Soc. Rev.*, 2021, **50**, 11530–11558.
65 Y. Fu, Y. Yao, A. C. Forse, J. Li, K. Mochizuki, J. R. Long, J. A. Reimer, G. De Paëpe and X. Kong, *Nat. Commun.*, 2023, **14**, 2386.
66 J. G. Vitillo and S. Bordiga, *Mater. Chem. Front.*, 2017, **1**, 444–448.

 This journal is © The Royal Society of Chemistry 2023